Journal of Building Engineering 86 (2024) 108936

Contents lists available at ScienceDirect

Journal of Building Engineering

journal homepage: www.elsevier.com/locate/jobe

Development of a foam-filled steel web sandwich panel for the rehabilitation of timber floors

Guilherme Gontijo [a], Marco Abreu Filho [a], Pier Giovanni Benzo [a], João M. Pereira [a,*], José Machado [b], Zlatan Z. Denchev [c], José Sena-Cruz [a]

[a] University of Minho, ISISE, ARISE, Department of Civil Engineering, Guimarães, Portugal
[b] FERPAINEL S.A., Braga, Portugal
[c] University of Minho, IPC-Institute for Polymers and Composites, Guimarães, Portugal

ARTICLE INFO

Keywords:
Sandwich panel
Thin-walled structures
Flooring design
Lightweight construction
Cold-formed-steel

ABSTRACT

Lightweight sandwich panels offer a prominent solution for the rehabilitation of timber floors. This paper addresses the development of a solution capable of continuous production for a foam-filled steel web sandwich panel for floor rehabilitation. The newly designed flooring solution is tested in full-scale quasi-static flexural campaigns. The tests validate the analytical design's compliance with Ultimate limit state (ULS) and Serviceability limit state (SLS) requirements. Furthermore, the flexural behaviour is compared with analytical predictions for thin-walled members according to the effective width method, described in Eurocode 3. Different effective cross-section design assumptions are assessed to allow an accurate prediction of the panel's response.

1. Introduction

Over the last decades, the reduction of environmental impacts and the development of technological innovations towards a more sustainable industry have been a growing concern worldwide. Within this context, changes to the construction industry are of key importance, since this sector is accountable for approximately 50% of all raw material extracted globally and generates 45–65% of the total amount of waste deposited into landfills [1,2]. In Europe, it is estimated that this sector is responsible for 50% and 40% of energy and raw material consumption, respectively [3].

The sustainable development of building solutions stands out as one of the main factors to currently drive the decision-making throughout the construction industry [3,4]. This involves making modifications, substitutions, or extensions to foster sustainable features on different constructive practices, addressed both for new engineering works as for the rehabilitation of existing buildings [5]. In fact, rehabilitation of old buildings is a growing concern at European level, since around 40% of the existing European buildings are dated before 1960, from which a substantial part was constructed with masonry and timber solutions [6,7]. In terms of structural performance, these buildings have already exhausted their nominal service life (50 years) requiring major maintenance and/or intensive rehabilitation procedures [7,8].

One key factor when dealing with the rehabilitation of masonry building concerns degraded flooring systems. The most common flooring system found in this kind of buildings are timber floors [9]. The simple replacement for a similar timber floor may not be the most suitable solution, as this system may not be able to attain current structural performance specifications or may require frequent

* Corresponding author.
E-mail address: jpereira@civil.uminho.pt (J.M. Pereira).

https://doi.org/10.1016/j.jobe.2024.108936
Received 30 October 2023; Received in revised form 12 February 2024; Accepted 25 February 2024
Available online 27 February 2024
2352-7102/© 2024 The Authors. Published by Elsevier Ltd. This is an open access article under the CC BY license (http://creativecommons.org/licenses/by/4.0/).

maintenance procedures to avoid excessive deformations over time [9–11].

In this context, the use of prefabricated structural elements arises as a highly prospective solution to contribute towards a more sustainable construction, especially due to the mitigation of environmental impacts by providing: i) savings on the construction time; ii) effective management of waste; and iii) simplicity of construction techniques [4,12–15]. In recent years, interest in prefabricated lightweight sandwich panels has increased due to their high stiffness-to-weight ratio [16]. A typical sandwich panel is composed of two thin skins with a low-density core between them [17]. Usually, the skins are made of fibre-reinforced polymers (FRP) or steel [18,19], and the core made of cellular foams or balsa wood [18,20].

Currently, most applications of steel sandwich panels are left to secondary elements or non-structural purposes. This is due to the sensitivity of thin-walled steel elements to premature buckling and instability phenomena, which can considerably compromise their structural safety [15,21–25]. Nevertheless, the innate high bending stiffness of sandwich panels can be associated with techniques to increase their buckling shear strength (such as the use of vertical webs or thin-walled joists, shear connectors or reinforced with concrete or composite elements) and therefore lead to their application in primary structural elements [21,26–34].

As a primary lightweight structural solution, one of the most promising applications for sandwich panels includes flooring decks used as modular constructive systems, since transport requirements imposes weight restrictions [35]. Ryu et al. (2018) [36] developed a sandwich panel-based flooring system composed by steel plates infilled with a high-density synthetic polymeric material, and the incorporation of a wire mesh for strengthening flexural strength under fire conditions (placed between the interface of the bottom steel plate and the core) and hollow core balls for reducing the polymer weight were assessed. All tested panels exhibited a satisfactory post-peak ductile behaviour and structural integrity under flexural loading [36]. Park et al. (2022) [37,38] have investigated the vibration response and the fire-resistance of steel-polymer sandwich panels used as flooring solutions. Besides an adequate fire and functional performance, the research revealed that the panels can also be incorporated with phase-change-materials into the polymeric core to enhance their thermal and fire performance [37].

Recently, several researchers have also developed flooring solutions comprising fibre-reinforced-polymers (FRPs) as face material, in association with several different core materials. Abdolpour et al. (2016) [39] investigated the use of GFRP sandwich panels infilled with PUR foam on the development of lightweight floor modules applicable in emergency dwelling in disaster areas [39]. Zhao et al. [40] investigated the mechanical behaviour of sandwich panel decks composed by glass-fibre-reinforced polymer (GFRP) and hybrid PUR foam core, in which different densities of PUR foam were used in association as core material to increase the shear capacity of the conceived flooring solution [40]. Similar strategy had already been used by Keller et al. (2008), but for GFRP sandwich panels used for a roofing application in Switzerland [41].

In this sense, a lightweight floor system built from sandwich panel arises as an interesting alternative for the rehabilitation of masonry buildings in old constructions [18,42–44], once it does not add significant dead load to the structure [16,45]. Therefore, the seismic response of these buildings, known to be vulnerable to extreme events, would remain unchanged or even improved, since the target of the panels is to keep similar levels of inertial forces and diaphragm stiffness as the previously existing timber floors [10,46,47].

This work falls within the scope of the Lightslab Research and Development project, that aims at the development of an alternative flooring system to current solutions, such as reinforced concrete and composite slabs, for application as a structural element in modular construction and on the rehabilitation of degraded timber floors. The main objective of the project is to conceive a cost-competitive lightweight system, based on cold-formed-steel sandwich panels, that allows greater efficiency and simplification of construction technology and ease of incorporation of installations (e.g. electrical, communications, water). Furthermore, this system is not subjected to biological attacks, and allows a direct and easy mechanical connection to existing masonry structures using steel angles which ease installation and maintenance procedures.

Within this paper, critical aspects regarding the development of a solution, capable of continuous production, of an innovative foam-filled steel web sandwich panel are assessed. Furthermore, an experimental characterization of the flexural response of the conceived panels was carried out. Additionally, a brief description of the analytical design of the sandwich panel will be presented, and in a final stage, compared to the obtained results for the full-scale tested prototypes.

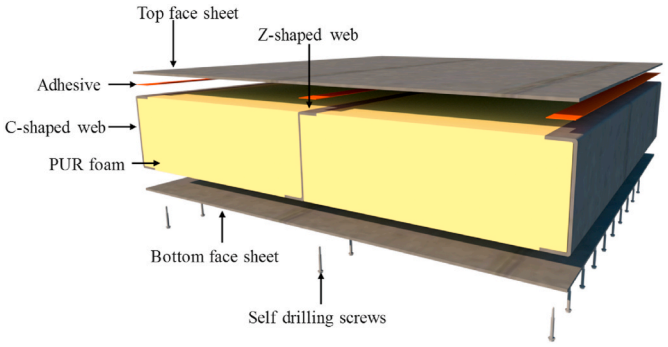

Fig. 1. Initial cross-section proposal of the cold-formed-steel sandwich panel [48].

2. Conception and analytical design of the cross-section

Within this research, a cold-formed-steel based sandwich panel (Fig. 1) was conceived and designed [48] to be used as a modular flooring solution and for the replacement of degraded timber floors, in applications such as the rehabilitation of masonry construction. The sandwich panel has a top and bottom face sheet that are made of cold-formed steel (CFS) sheets with nominal thickness of 1 mm. The vertical webs are also CFS C-sections and Z-sections. The cavities between the webs are filled with polyurethane foam (PUR) with a nominal density of 40 kg/m^3. Although several experimental and analytical studies suggest that the presence of a cellular core enhances the local instability resistance of the sandwich panels [24,49,50], the design of the flooring system was conducted in a conservative approach, disregarding the foam mechanical contribution. Therefore, the panel was assumed as a hollow built-up cold-formed-steel (CFS) cross-section. The overlapping parts of the flanges and face-sheets were considered jointed in the adhesive area's mid-line. The overhanging part of the flanges was regarded as an outstand element, whereas the part between the web and the adhesive mid-line was regarded as an internal element [48]. Such definitions are necessary to calculate the slenderness and cross-section area reduction due to local buckling. According to the Euler-Bernoulli beam formulation, the structural model adopted is a simply supported beam with a fixed span length and subjected to a uniformly distributed load, as detailed in Annex A.

Although the use of built-up CFS sections is currently accelerating due to the growing use of CFS elements in general construction applications [51], building codes in general do not provide information on the design of CFS built-up section members. Thus, several researchers have proposed and validated different methods to conduct their design. According to Xu et al. [52], the flexural capacity of a built-up box section subjected to concentric loading may be obtained by application of the superposition method, in which the sum of the capacity of the individual members yields the strength of the entire built-up section [52]. Li et al. [53] compare the prediction of the flexural resistance of a built-up box beam bending about its weak axis against experimental results. The effective width method (EWM) described in the Eurocode 3 [54] is used to predict the flexural strength by considering an equivalent simplified box section. The technique is deemed reliable for cross-sections with a width-to-thickness ratio not greater than 100 [53]. Yao et al. [55] conducted a comparison between the experimental flexural strength of a built-up box section bending about its strong axis and the analytical prediction obtained through the EWM as described in the American and Chinese building codes (AISI S100–2016 and GB 50018-2002, respectively [56,57]). The former is considered too conservative, while the latter is unconservative [55]. Regarding the deflection prediction at the Serviceability limit state (SLS), Ye et al. [58] compare the results of the flexural tests on back-to-back built-up channel sections with analytical predictions obtained by different methods. Considering the gross-cross-section properties leads to an underestimation of the deflection of about 8%. On the other hand, the interpolation method of the Eurocode 3 is deemed the most reliable, with a slight overestimation of the vertical deflection [54,58].

The resistance verifications for the proposed sandwich panel flooring solutions to the design actions at the Ultimate limit state (ULS) were performed for the most typical failure modes of thin-walled CFS profiles. These include bending moment analysis considering buckling due to local instability of the individual plates and shear buckling of the panel webs. The effective width method (EWM), described in Eurocode 3 – Parts 1–3 and 1–5 was used to estimate the load-bearing capacity of the sandwich panel [54,59]. This method adopts an iterative procedure to determine an equivalent area of all the plates of the cross-section accountable for the ensued longitudinal stresses after local buckling of the steel occurs. Thus, it allows for the calculation of the load-bearing capacity of the panels with respect to bending moment (M_{Rd}) and shear (V_{Rd}), according to Equation (1) and Equation (2).

$$M_{Rd} = \frac{W_{eff} \times f_y}{\gamma_{M0}} \tag{1}$$

$$V_{Rd} = \frac{n_w \times h_w \times t_w \times f_{bv}}{\gamma_{M0}} \tag{2}$$

where W_{eff}, h_w, t_w and n_w are geometrical parameters related to the cross-section (effective section modulus, height of the webs, thickness of the webs and number of webs, respectively) and f_y, and f_{bv} represent the nominal value of the yield strength as prescribed by the Eurocode 3 Part 1–3 and the shear strength considering buckling, respectively [54]. γ_{M0} is a partial factor for the resistance of the cross-section, set as 1.00 for the current application [54]. The obtained load-bearing capacity is then compared with the ULS load action combination, determined according to EN 1990 and EN 1991-1-1, and described in detail in Annex A [60,61]. With regards to Serviceability limit state (SLS) verification, the coding establishes a maximum deflection of the structure when subjected to SLS load combination (δ_{max}) as a ratio of the clear span length (L), as shown in Equation (3) [54]. Additionally, the Eurocode 3 establishes a maximum deflection due to variable actions (δ_2), as shown in Equation (4) [54]. Further details are reported in Annex A.

$$\delta_{max} \leq \frac{L}{250} \tag{3}$$

$$\delta_2 \leq \frac{L}{300} \tag{4}$$

The Portuguese National Annex in NP EN 1993-1-1 require verifications against excessive vibrations if the vertical deflection (δ_{max}) is higher than 28 mm [62]. For the current application, since the maximum studied span length is 5.0 m, the fulfilment of Equation (3) imposes that the deflections may not be higher than 20 mm, which correspond to a more stringent limit for the SLS deflection and therefore allows disregarding the verifications against vibrations.

Besides the structural verifications, the design of the panel was also conducted to ensure an adequate thermal and acoustic

functional response. In this regard, a metaheuristic genetic algorithm was adopted, to pursue for design solutions that attain structural, and a fraction of functional requirements set by building codes (which will be complemented by additional insulation layers on the final solution), minimizing cost, mass, and carbon-footprint of the flooring system [48]. This algorithm thoroughly assessed different cross-section geometries considering a fixed clear span length of 5.0 m, by varying the following factors: i) total thickness of the panel, thickness of the steel face sheets; ii) width of the web flanges; iii) number of intermediary webs and iv) density of the polyurethane foam used as core material. The technical details regarding the implementation of the genetic algorithm, a comprehensive description of the effective width method (EWM) used to estimate the load-carrying capacity of the panels and the obtained optimized solutions for each one of the targets are fully reported in Ref. [48]. The optimal cross-section architecture obtained after the optimization campaign is shown in Fig. 2.

3. Practical aspects of the manufacturing process

The manufacturing process of the optimized sandwich panel flooring system in a continuous production line consists of the following steps: i) slitting of the steel coil which will be used as a bottom face sheet of the panels; ii) placement and fixing of the C and Z-shaped vertical elements (webs) to the bottom face sheet of the panel (Fig. 3a); iii) slitting of the steel coil that will be used as upper face sheet of the panels (Fig. 3b); iv) application of the polyurethane-based structural adhesive to the top face of the webs (Fig. 3c); v) injection of the liquid polyurethane (PUR) into the bottom face sheet, which polymerizes and cross-links expanding into a foam that fills the cavity constrained by the webs, creating a strong bond between the steel elements and the foam core (Fig. 3d); vi) placement and adhesively bonding of the upper face sheet to the webs; vii) subjecting the panels to a brief curing process (42 °C for 7 min, directly after foaming), to ensure that the foam expands uniformly and adheres tightly to the steel sheets and enhance the bonding of the polyurethane-based adhesive [63,64]; viii) cutting and trimming of the panel into the desired length (Fig. 3e). The final aspect of the sandwich panels at the end of the production line is shown in (Fig. 3f).

The main practical challenges associated with the implementation of a continuous production line for such panels are related to the placement and fixing of the C and Z-shaped vertical webs to the bottom face sheet (step ii), which, due to their slenderness (and consequent low rigidity), are prone to misalign, deform and buckle during their assembling and/or injection of the liquid PUR (Fig. 4a). Eventual misalignments and deformations represent a huge setback for the panels, once initial imperfections can contribute to premature yielding of the thin-walled CFS members, which have their failure primarily governed by local instability phenomena [58,65,66]. Furthermore, with current production machines the intermediary vertical elements (Z-shaped webs) at the cross-section of the panel affect the formation and stabilization of the PUR foam, leading to the occurrence of voids and heterogeneities in the core (Fig. 4b). Although these issues could be solved by the manual assembling and foaming of the sandwich panels or with major modifications on the production line, this would lead to a significant reduction on the efficiency of the productive process, which considerably compromises the economic feasibility of the flooring solution.

Therefore, an alternative geometric design was conceived to tackle these problems (Fig. 5a). In this configuration, there is no need to position and fix any type of C or Z-shaped profiles on the panel faces, since the webs consist of lateral reinforcements (stiffeners) obtained by folding the lower steel face sheet, which was also conceived to ensure a better fit between adjacent panels. The width of the panels, in this version (0.5 m), would necessarily have to be smaller than the width of the prototypes previously designed in the project (1.0 m), which, on the other hand, mitigates the need for intermediary webs and thereupon contributes to a more homogeneous stabilization of the PUR foam core. For the alternative geometric cross-section, the sandwich panels were designed for a clear span of 4.0 m, which although smaller than the clear span considered in the optimization campaign (5.0 m) described in section 2, still correspond to the average span length identified in old masonry buildings across Portugal and Europe, as illustrated in Fig. 6b [48,67]. Furthermore, the panel can still be easily adapted for higher span lengths by incrementing its nominal thickness of the built-up CFS elements or its overall height, if required for specific applications [68].

Considering that in a first stage the production of this prototype took place manually, the lower steel face-sheet had to be previously shaped to the intended configuration (Fig. 5b), using a profiling bending machine, and then inserted directly into the production line for foaming and adhesive joining of the top face sheet (Fig. 5c).

Having in mind the future objective of automating the production process, changes would have to be made to the profiler to fold the sheets unwounded directly from the coils. From a practical point of view, with the adoption of the profilers to obtain the desired shape for the face sheet of the panel, the continuous production of this flooring solution with adequate dimension consistency and quality control is deemed highly feasible. A schematic of a 3D representation for the possible application of the developed flooring solution is

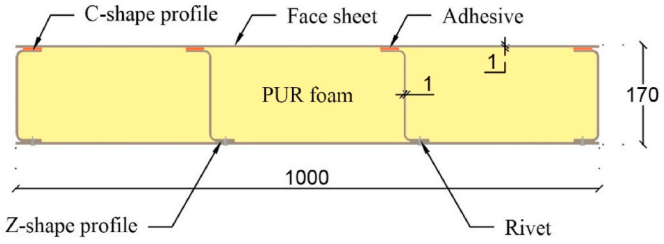

Fig. 2. Sandwich panel cross-section obtained with genetic algorithm [48].

Fig. 3. Example of the manufacturing process of the prototype sandwich panel: a) placement of vertical elements (webs); b) bottom and top face sheet on production line; c) adhesive on top of web and uncoil of upper face sheet; d) injection of the liquid PUR compound that forms the foam; e) placement of panel in packaging line for cutting/trimming; f) final aspect of the manufactured panel.

shown in Fig. 6a, whereas the cross-sectional view of the sandwich panel system is shown in Fig. 6b.

4. Experimental program

After the successful manufacture of the prototypes shown in Fig. 5, six panels with 2.0 m length were produced for a preliminary experimental campaign, carried out with the following objectives: i) assess the flexural response of the flooring solution and verify the analytical design compliance with Ultimate limit state and Serviceability limit state requirements; ii) identify failure modes and their propagation; iii) evaluate the mechanical behaviour of adhesively connected adjacent panels. Within this campaign, the panels were tested in a four-point bending configuration, whereby two tests were carried out in individual panels and two more tests were performed in sets of two adhesively jointed panels (slabs).

The jointed panels were bonded using an epoxy structural adhesive (S&P Resin 220 HP), applied on the surfaces to be bonded after mechanically treating the latter with sandpaper and cleaning with acetone. The jointed panels were properly attached using ratchet tie-down straps and left to cure for 72 h at room temperature prior to removal of the straps and initiation of the experimental campaign. To assure an efficient load distribution among the two connected panels, a thin layer of bitumen-based polyester putty was applied for the rectification of the load application zones.

For the tests, the panels were placed over a pin and a roller supports, to reproduce a simply supported configuration with a clear span of 1.80 m length and a shear span of 0.60 m, and metallic spreader I-beams were used to uniformly distribute the force from the actuator within the two loading zones. The test setup is shown in Fig. 7.

Throughout the test, the deflections were measured using RDP-ACT-Series LVDTs positioned under the loaded section (75 mm range, with linear error of ±0.075 mm) and at midspan cross-section (100 mm range, with linear error of ±0.1 mm). Furthermore, two auxiliary bars were attached to the lateral faces of the sandwich panels at the support areas, and LVDTs were installed on it to measure the vertical deflection disregarding eventual displacements which may occur on the panels due to the settlement of the supports. Additionally, Tokyo-Measuring PFL10-11 strain gauges (SG) were placed at the top and bottom face sheet of the sandwich panels (gauge length of 10 mm, gauge factor of 2.12 and transverse sensitivity of ±0.5%). A schematic of the lateral view of the

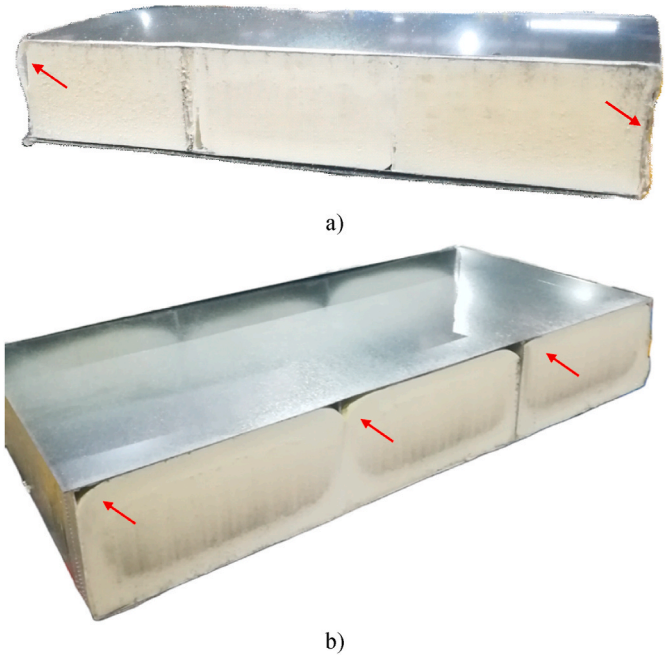

Fig. 4. Practical challenges observed on manufacturing trials of prototypes with C and Z-shaped elements as webs: a) buckling/misalignments on the webs; b) voids in the PUR foam core.

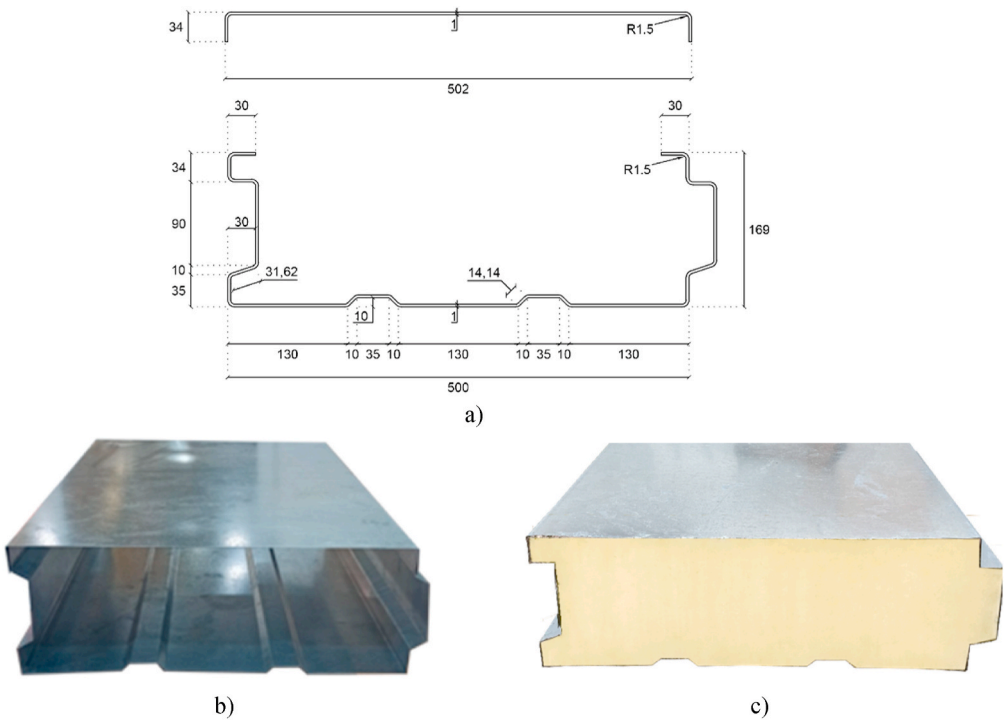

Fig. 5. Geometry of the alternative prototype: a) geometric dimensions; b) cold-formed-steel built-up cross-section; c) panel after core foaming and bonding of face sheets.

instrumentation used on the tests in represented in Fig. 8a, whereas the cross-section for both the individual and jointed panel configurations are shown in Fig. 8b and c, respectively. Data was collected throughout the entire tests at a frequency of 4 Hz. All the tests were conducted at the Structures Laboratory of the Civil Engineering Department at University of Minho, in quasi-static monotonic-

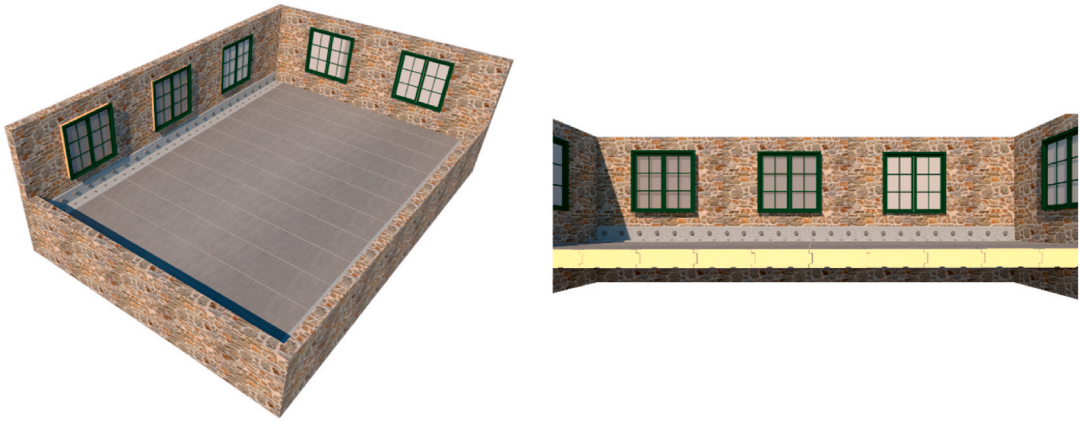

Fig. 6. Schematic of potential application of the flooring solution: a) 3D representation; b) cross-sectional view of the sandwich panel system.

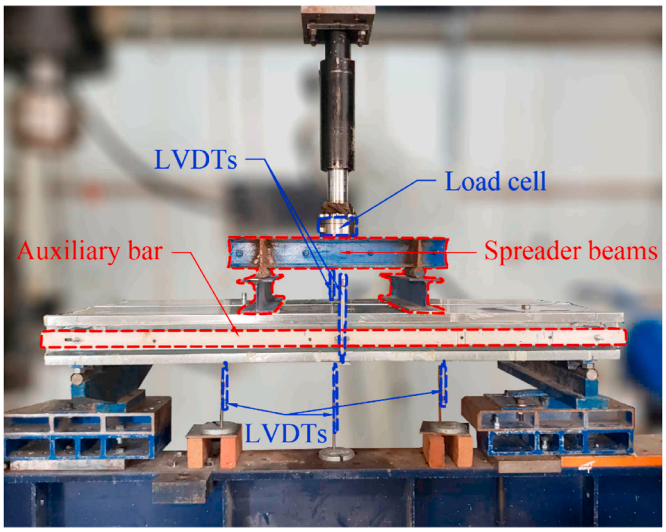

Fig. 7. Test setup used on flexural four-point-bending tests.

instantaneous loading up to failure, under displacement control at a rate of 1.8 mm/min applied using an AEP-TC4 force transducer load cell (nominal load of 200 kN ± 0.3 kN).

5. Experimental results & discussion

As mentioned before, two experimental campaigns were performed to assess the flexural behaviour of the developed sandwich panels: a) single panels; b) jointed panels. The obtained results are shown and thoroughly discussed for each of these sets within the following subsections.

5.1. Single panel flexural test

As reported in section 4, two sandwich panel prototypes were tested under quasi-static four-point bending tests. The evolutions of force *versus* average midspan deflection and strain measurements, respectively, are shown in Fig. 9a and b. The average of the vertical displacements measured by the two LVDTs installed on the auxiliary bars and located at midspan were considered for the calculation of the midspan deflection shown in Fig. 9a, in order to monitor the bending component of the panel deflection disregarding settlements and deformations at the support regions.

In general, the panels exhibited a consistent behaviour in terms of flexural stiffness, with a slight difference of strain evolution. From the beginning of the test, the strains evolved linearly both at the top and bottom face sheets of the panel, which correspond to compressive and tensile zones, respectively. Then, with the onset of local instability phenomena, non-linearities are observed in the evolution of strains. Specifically at the top face sheet, the initiation and progression of wrinkling causes the maximum compressive

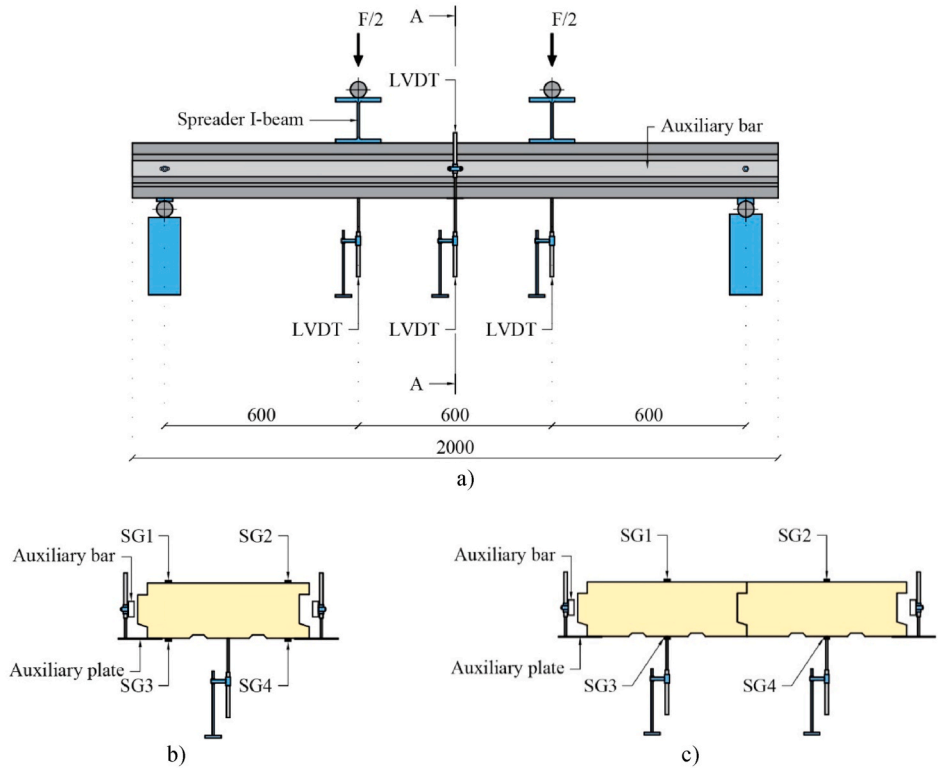

Fig. 8. Schematic of instrumentation used on four-point bending test: a) lateral view of overall test setup; b) single panel cross-section; c) jointed panels cross-section.

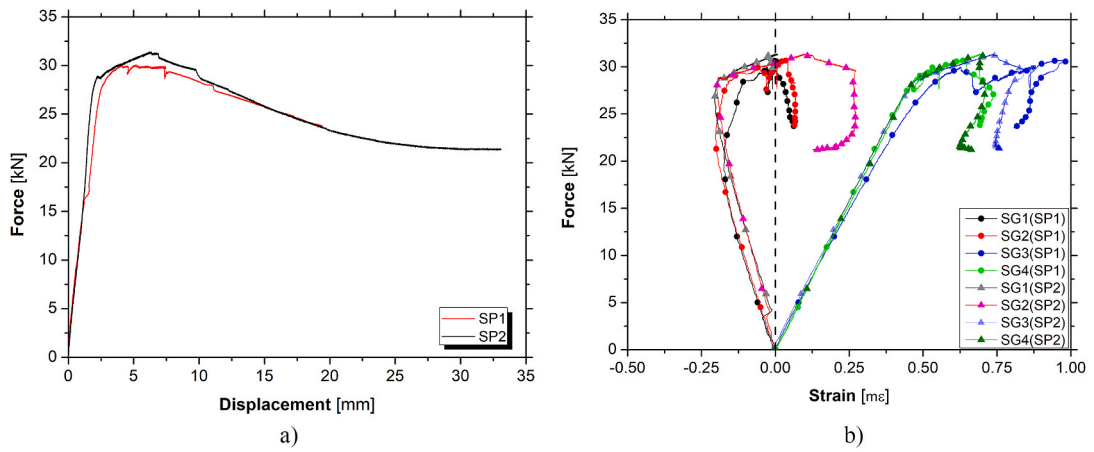

Fig. 9. Measurements during single panels flexural test: a) force versus average midspan deflection; b) force versus strain evolution.

strain to be recorded before the ultimate load. The onset of this phenomenon can be prematurely triggered and intensified by eventual initial geometric imperfections in the tested specimens. After this stage, strain gauges recorded the elongation of the steel member, with a transition from negative to positive strain measurements.

For the bottom face sheet, the tensile strain evolution starts with a linear response, followed by a non-linear branch until peak load is reached. After peak load, the strains still increase within negative values until the support zones are considerably affected by plastic deformation phenomena, reaching values from 0.7 to 0.9 mε followed by a strain decrease. This range of strains correspond to the onset of non-linearities observed within the tensile characterization of CFS coupons for the assessment of their engineering properties, reported in detail in Ref. [69].

As expected, in a first stage both panels have shown a linear elastic behaviour, followed by a nonlinear branch due to plastic deformation resulting from the wrinkling of the upper face sheet of the panels. In both tested panels, wrinkling was followed by progressive deformations on the vertical element of the web adjacent to the upper face sheet on the loading zone.

For panel SP1 test (Fig. 10), after wrinkling started to occur (Fig. 10a), plastic deformations were also triggered in one of the support regions, which gradually progressed until the complete crushing of the vertical elements of the web adjacent to the bottom face sheet of the panel due to shear buckling (Fig. 10b). It is worth noticing that, although the bottom part is stiffer than the upper face sheet of the panels, the indentations (stiffeners) on the bottom face reduce the contact area between the support and the panel, which can contribute to a higher concentration of stresses and consequent strains on the surroundings of this contact area. Moreover, the edges of the top face sheet at the cross-section are composed by an overlapping region with the web cores, which improves the stiffness of the top part of the panel. Finally, a high concentration of plastic deformation also took place on the webs due to shear stress concentration at one of the loading zones (Fig. 10c).

In panel SP2 (Fig. 11), nonlinearities also initiated with the wrinkling of the upper face sheet on the edges of both loading application zones (Fig. 11a), then, deformation appeared on the vertical elements of the webs adjacent to the upper face sheet (Fig. 11b), which occurs at the ultimate load and thereupon leads to the initiation of the load decrease. This phenomenon was more accentuated in one of the loading zones, causing shear buckling throughout the entire web and ending with the formation of a plastic hinge at the fully deformed web with a tilted aspect (Fig. 11c). For panel SP2 no major deformations were noticed at the support regions.

Comparing the aspect of both tested panels at the end of the tests (Figs. 10c and 11c) it is noticeable that in SP1 the plastic deformations were distributed between one of the loading zones and the opposite support, while in panel SP2, plasticity mostly occurred within the region of a single loading zone. This aspect reflects on the overall load (and consequent strain/plasticity) distribution, which is highlighted by the tilted aspect of the spreader beam at the end of the test on panel SP2, as a consequence of the formation of a plastic hinge in one of the loading zones (Fig. 11c).

5.2. *Jointed panel flexural test*

The flexural response of two sets of adhesively jointed panels was also tested in quasi-static four-point bending tests. Although the

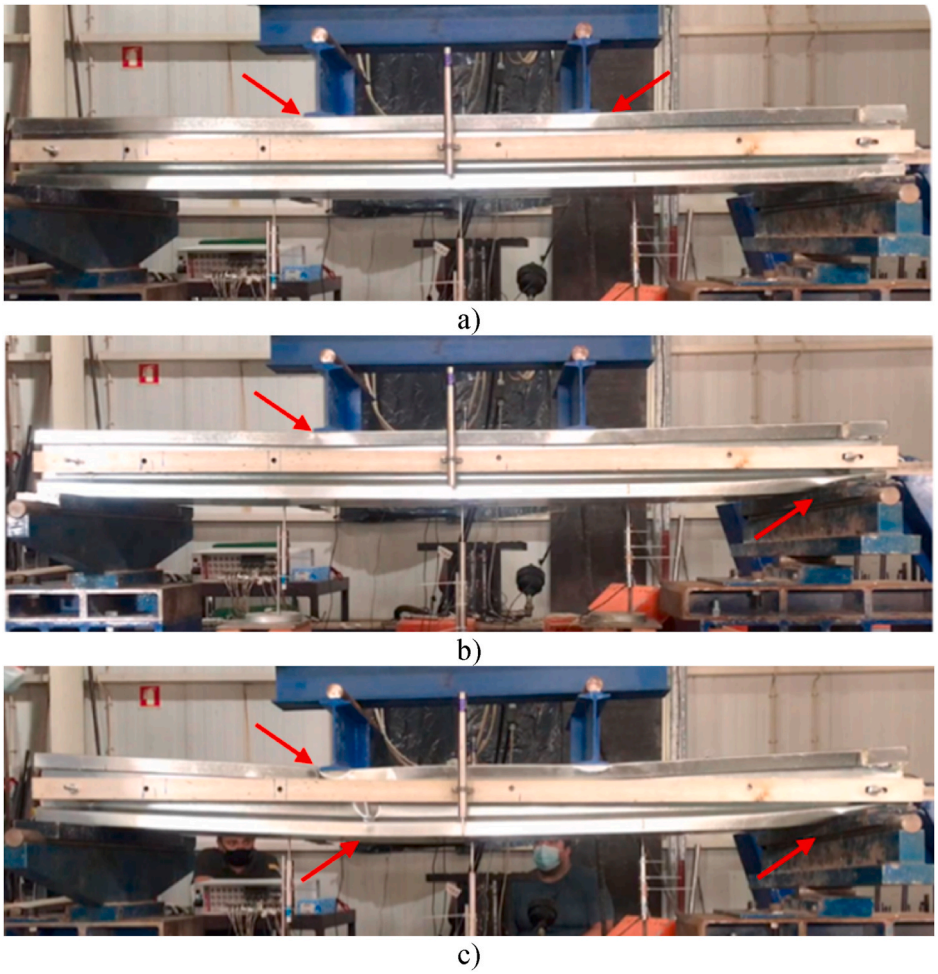

Fig. 10. Evolution of flexural test on SP1: a) wrinkling of the upper face sheet; b) shear buckling at vertical elements of web at the support; c) buckling of the web at loading zone.

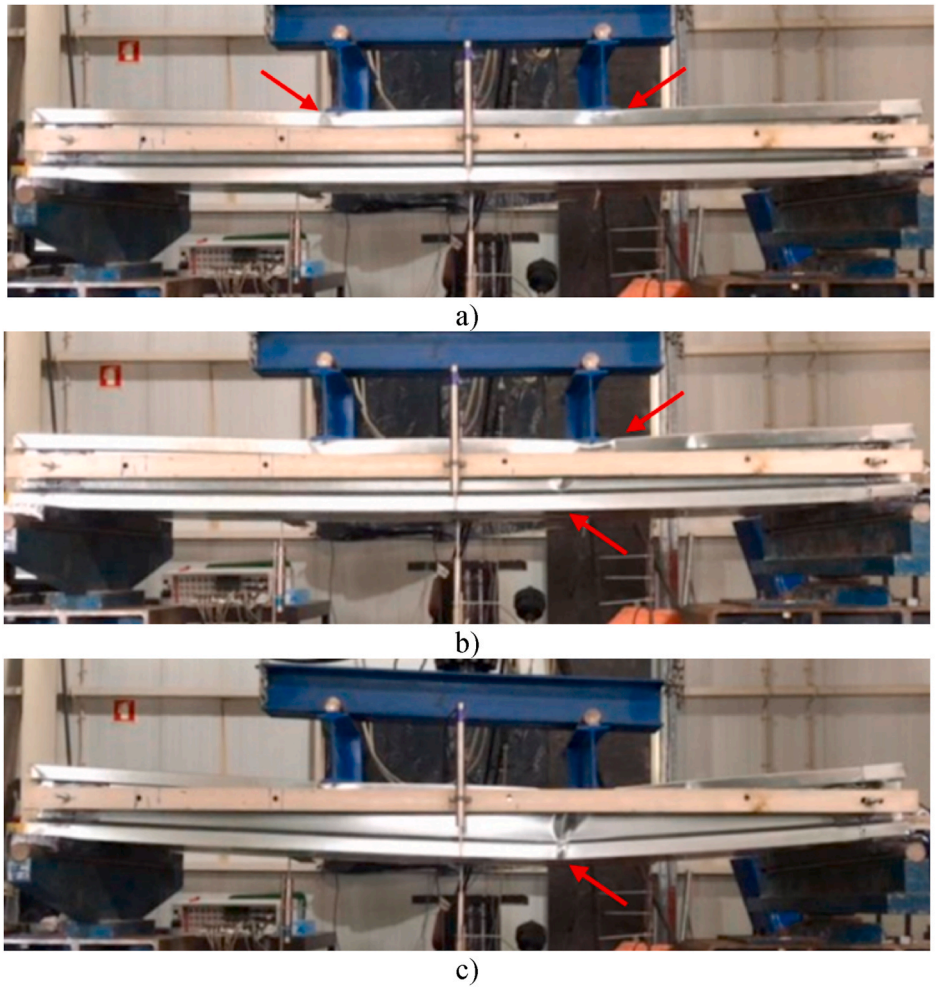

Fig. 11. Evolution of flexural test on SP2: a) wrinkling of the upper face sheet; b) shear buckling on the web at loading zone; c) formation of plastic hinge.

failure modes observed on these tests were also related with local instabilities on the face sheets and excessive deformations due to shear buckling of the webs (at the loading zones but specially at the supports), the panels exhibited a different force *versus* average midspan deflection and strain evolutions, as shown in Fig. 12a and b, respectively.

Initially, the strains gauges recorded an increase of compressive and tensile strains within the top and bottom steel elements

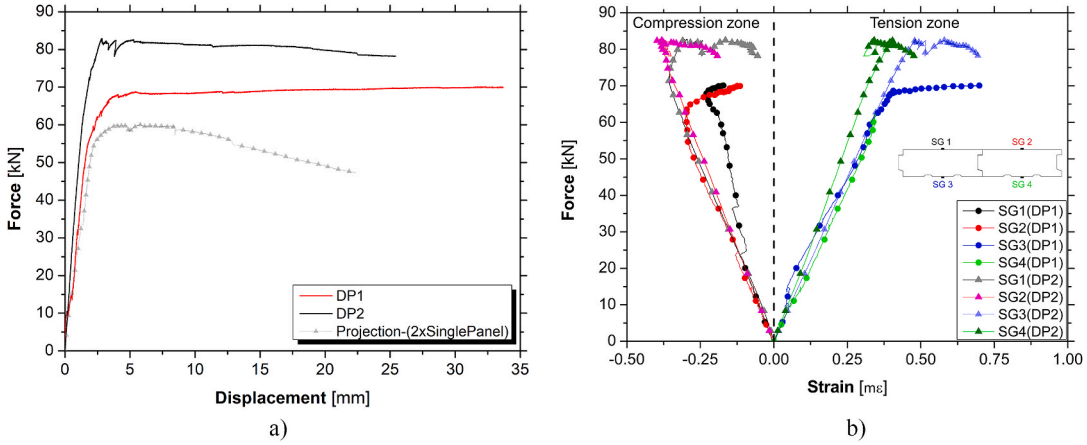

Fig. 12. Measurements for jointed panels flexural test: a) force versus average midspan deflection; b) force versus strain evolution.

respectively. With regards to strain evolution and failure modes, as for the individual tests, in both sets of jointed panels the nonlinear behaviour initiated with the wrinkling of the upper face sheet. Nevertheless, for set of panels DP1, wrinkling (Fig. 13a) was firstly triggered in one of the panels, which led to an uneven distribution of strain among the jointed sandwich panels, noticed specially for the top face sheet. This aspect reveals that the two panels were not equally affected by instability phenomena. Consequently, plastic deformation occurred both at the loading zone and at the supports in one of the jointed panels, which were already initially damaged when deformations started to occur on the loading zones and supports of the next. This uneven strain distribution is evidenced by the behaviour presented by SG1, which approximately at 25 kN already started to exhibit non-linearities due to local buckling, while SG2 preserved a linear response up to more than 50 kN, as shown in Fig. 12b. Although SG4 stopped recording at approximately 60 kN of load (possibly due to detachment or damage on the strain gauge cables), the two strain gauges placed on the bottom face sheet of the panels have shown a consistent strain evolution throughout the loading of the panels for set DP1.

In other words, in terms of failure progression set of panels DP1 behaved as two individual sandwich panels rather than as a jointed slab. Nevertheless, the tested prototype still exhibited an adequate structural response, preserving its full load-bearing capacity even after intense plastic deformations. In fact, the load-bearing capacity of the panel kept slightly increasing throughout the entire test, even after progressive crushing of the vertical webs adjacent to the bottom face sheet at the supports (shown for each of the supports in Fig. 13b and c). This aspect may be related to the non-occurrence of prominent buckling failure at the webs on the loading zones, which as observed for the individual tests, corresponds to a sudden drop on the load-bearing capacity of the panels.

For set of panels DP2, after wrinkling of the upper face sheet, plastic deformation also started to occur at the webs adjacent to the bottom face sheet in one of the support regions (Fig. 14a). Concomitantly to the deformation and posterior crushing of this support area, plasticity also progressively evolved through the elements of webs adjacent to the upper face sheet at the opposite loading zone of the panel, as shown in Fig. 14b and c. Although at the end of the test both supporting regions were deformed, the crushing of the vertical elements at the webs only took place in one of the supports. For the set of panels DP2, the load and plasticity phenomena were distributed in a more homogeneous way, as can be observed by the compatible behaviour shown by the strain gauges (Fig. 12b) specially at the top face sheet of the panels. Although a slight difference was noticed on the behaviour of SG3 and SG4 for this set, both placed at the bottom face, this aspect did not visually affect the failure evolution between the panels throughout the test.

As seen in previous tests, the onset of wrinkling is influenced by the presence of geometric imperfections. The propagation of this phenomenon influences the evolution of failure mechanisms as the load increases during the tests. The different strain and failure evolution observed especially at the compression zones led to the lower ultimate load observed for set of panels DP1, when compared to set of panels DP2. This variability is related to an inefficient compatibility of deformations by the connection for set of panels DP1, highlighted by the different behaviour exhibited by the strain gauges placed on the upper face sheet each of the connected panels.

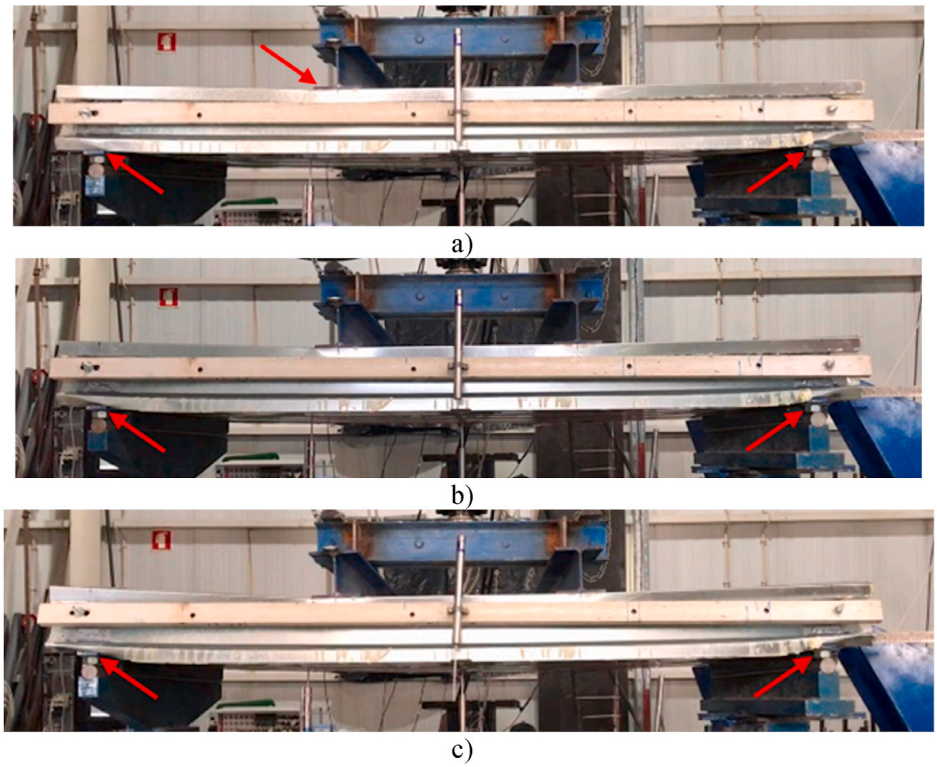

Fig. 13. Evolution of flexural test on DP1: a) wrinkling and initiation of plastic deformation at the supports; b) crushing in one of the webs at the support region and evolution of plasticity on the opposite; c) shear crushing of webs at both supports.

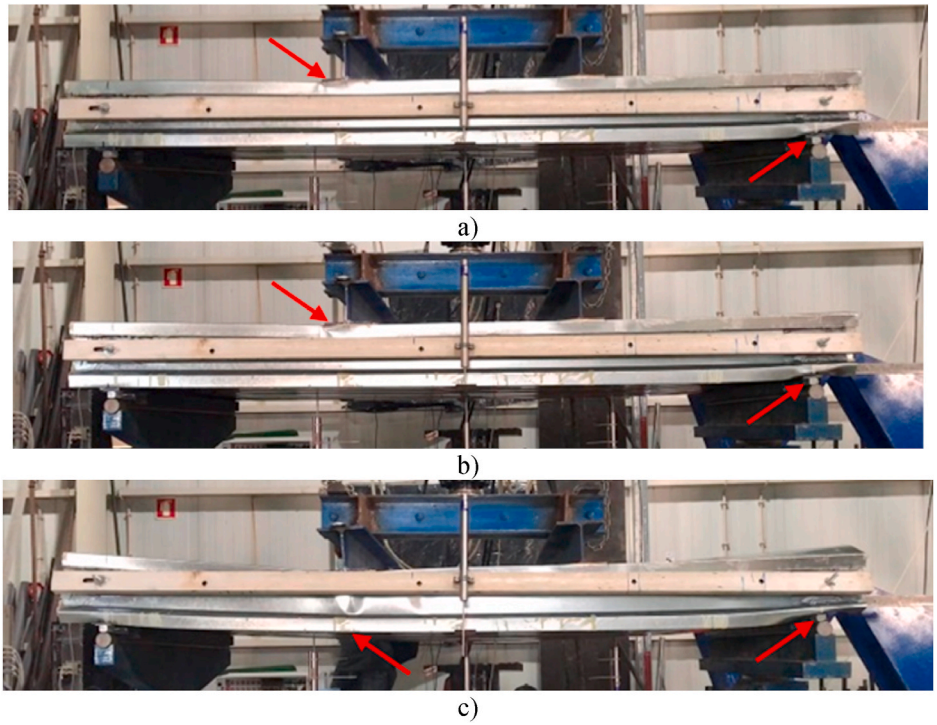

Fig. 14. Evolution of flexural test on DP2: a) wrinkling and plastic deformations at one of the supports; b) shear crushing at the web of a support and initiation of plasticity at the opposite loading zone; c) buckling of the web at loading zone.

Besides the eventual presence of initial imperfections, parameters such as the effective thickness of the adhesive connection may be associated to the variability in the results.

Despite the differences identified on the jointed panel tests, the flexural load-carrying capacities obtained for both sets are higher than 2 times the experimental strength observed for a single panel, as shown in Fig. 12a, showing some beneficial synergic effects. Likewise, on the connected panels a smaller decay on the flexural stiffness after initiation of local buckling was noticed (specially for set of panels DP2). This indicates that an efficient panel-to-panel connection can contribute to a more compatible strain distribution and postpone the evolution of failure due to instabilities throughout the CFS members. These aspects are also related to the intersection of the two jointed webs at the middle of the cross-section, which act as a less slender CFS thin-walled member (since it has twice the thickness of a single web), and therefore is less susceptible to premature yielding due to local instability phenomena. Moreover, both sets of jointed panels exhibited a satisfactory load-carrying preservation after damage due to progressive plasticity.

6. Comparison of experimental results and analytical design

According to the Eurocode 3 Part 1–3 [54], the ultimate load-carrying capacity of the sandwich panel (F_{ULS}) is determined using the EWM. F_{ULS} can be obtained from the bending moment resistance of the cross-section (M_{Rd}), as explained in Annex A. Table 1 compares the measured and calculated load-carrying capacity of the tested panels. The experimental ultimate load-carrying capacity of the panel (F_{EXP}) is 1.40 times the analytically predicted value. Other researchers showed that the ratio between the predictions based on the EWM and the experimental flexural resistance of hollow built-up CFS box section is generally about 1.0 [52,53,55]. Therefore, the bending stresses ensued throughout the test are deemed properly transferred between the two CFS face sheets. Furthermore, the obtained results emphasize that neglecting the contribution of the PUR foam led to a conservative flexural strength prediction.

The analytical deflection estimated for SLS loading combination can also be compared with specific deflections measured directly on the flexural tests. Furthermore, the bending stiffness of the sandwich panels can be used to verify the effective width assumption, which postulates that a fraction of the cold-formed-steel cross-section should be reduced proportionally to the level of compression in the flanges and in the webs. The analytical calculations conducted to allow these comparisons are detailed in Annex A. In Fig. 15 the experimental results obtained for the single panels are plotted, as well as the maximum predicted force estimated by the analytical design for ULS and the equivalent SLS load level, both determined according to Eurocode 3 [54].

Therefore, in an attempt to quantify the contribution of the PUR foam to the structural performance of the CFS built-up members, three methods are considered for the estimation of the deflection at the SLS: i) Method 1 considers the gross cross-section properties along the length of the beam; ii) Method 2 considers the effective cross-sectional determined at the maximum stress level along the beam span; iii) Method 3 considers the variation of the effective second moment of inertia by using an interpolation between the gross cross-section properties and the effective properties determined at the maximum stress level.

Table 1
Comparison between ULS analytical design and experimental results.

Specimen [−]	M_{EXP} [kN·m]	F_{EXP} [kN]	F_{ULS} [kN]	F_{ULS}/F_{exp} [−]
SP1	9.22	30.73	22.22	1.38
SP2	9.42	31.39	22.22	1.41
Avg	**9.32**	**31.06**	**22.22**	**1.40**

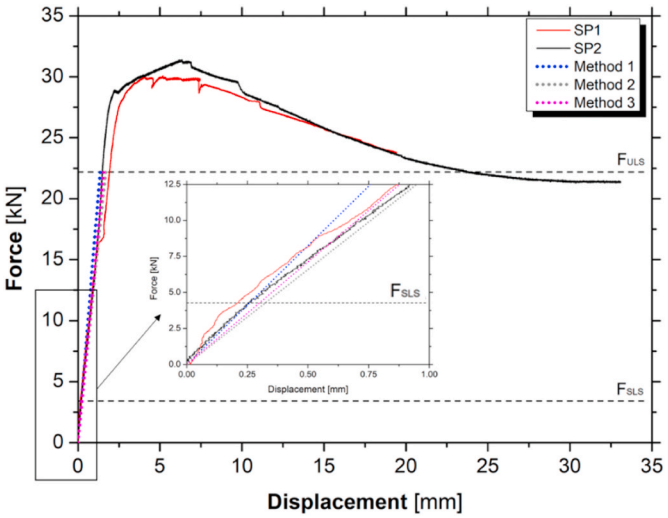

Fig. 15. Comparison of predicted SLS deflection and ULS load-carrying capacity based on analytical design and experimental results obtained for single panels.

Method 1 relies on the PUR foam being sufficiently rigid to prevent local instabilities in the plate elements of the cross-section. The yield stress in the extreme compression fibre of the sandwich panel is reached assuming an elastic distribution of stresses in the cross-section (see Fig. 16a).

Method 2 does not take into consideration the contribution of the PUR foam. Therefore, it assumes that local instabilities will occur before the cross-section develops its elastic moment resistance. These local instabilities cause an uneven stress distribution across the width of the plate elements. To address this issue, an iterative procedure is used to penalise the cross-section area until a compatible stress field and effective area are achieved (see Fig. 16b).

Method 3 follows the guidelines set out in Eurocode 3 Part 1–3 [54], which doesn't consider the impact of the PUR foam. However, the bending stress variation that causes local buckling is accommodated by calculating the effective cross-section properties at the midspan cross-section, where the maximum stress occurs, and interpolating them with the gross cross-section properties.

In summary, three methods are considered to evaluate the bending stiffness of the sandwich panel cross-section. Method 1 is the least conservative, as it assumes that the sandwich panel cross-section is equivalent to a hot-rolled steel section that can develop its full elastic moment resistance. On the other hand, Method 2 is the most conservative, as it assumes that the sandwich panel cross-section is equivalent to a CFS built-up member without filling. Method 3 represents an intermediate state between the previous two methods. The predicted bending stiffness in accordance with each of these hypotheses is also represented in Fig. 15.

Table 2 provides a comparison between the measured and calculated deflection at the SLS load level (δ_{SLS}) and elastic flexural stiffness (K) of the sandwich panels. The value of δ_{SLS} is determined from the load-displacement curve at the SLS load level, which is

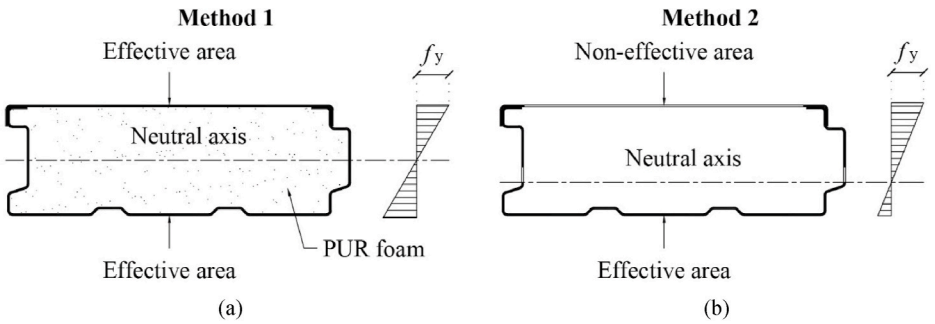

Fig. 16. Design method for the estimation of the sandwich panel's deflection: (a) Method 1; (b) Method 2.

Table 2
Comparison between SLS analytical design and experimental results.

δ_{SLS} [mm]	Analytical prediction [mm]			K [kN/mm]	Analytical prediction [kN/mm]		
	δ_{M1}	δ_{M2}	δ_{M3}		K_{M1}	K_{M2}	K_{M3}
0.20	0.21 (+6.5%)	0.26 (+31.9%)	0.24 (+21.7%)	11.8	16.5 (+40.4%)	13.2 (+12.3%)	14.2 (+20.9%)

Note: δ_{SLS} and K represent the average of the obtained for the two single panels tested. The values between parentheses are the relative difference between experimental results and analytical prediction.

estimated using the prescribed load combination in the Eurocode 0, and for the current case represent a distributed load of 2.80 kN/m^2 [60]. The details of the load combination are given in Annex A. The elastic flexural stiffness is calculated by determining the slope of the load-displacement curve in the load interval between 20% and 40% of the ultimate load registered. The expressions for calculating the analytical deflections (δ_{M1}, δ_{M2}, and δ_{M3}) and stiffness (K_{M1}, K_{M2}, and K_{M3}) based on the Euler-Bernoulli beam theory are provided in Annex A.

The curve obtained from Method 1 in Fig. 15 shows that considering the gross cross-section properties leads to a small overestimation of the vertical deflection at the SLS load level (about +6%). Ye et al. (2018) also compared the EC3 deflection predictions with the experimental deflection of a built-up box beam bending about its weak axis [58]. However, the study showed that considering the gross cross-section properties led to an underestimation of the deflection. Therefore, it may be concluded that the PUR foam is efficiently supporting the CFS face-sheet and contributing to uniformly distributing the bending stresses across the width of the cross-section. On the other hand, all assessed methods overestimate K for load level higher than the SLS. This may be due to the fact that the analytical model considers a perfect geometry. In the experiment, nonlinear geometrical effect may be already arising in the load range considered for the calculation of K.

Indeed, the experimental flexural stiffness obtained from the tests was calculated within a range from 20% to 40% of the ultimate load measured on the test. The lower limit is to avoid capturing eventual adjustments and settlements that occur with the initiation of the test, while the upper is adopted to disregard eventual non-linearities and deformations that may occur due to early yielding or plasticity effects on the sandwich panels at higher loads. Nevertheless, premature plasticity due to instabilities is highly sensitive, and thereupon may be already taking place at a certain level within the considered load range.

From the comparison between analytical predictions and the experimental results, Method 1 led to the smaller relative error on the estimation of the deflection within the SLS load level (+6.5% relative difference). Neglecting the stabilizing effect against buckling of the PUR foam results in much more conservative predictions. On the other hand, for load levels higher than the SLS load level, Method 2 has yielded the most accurate predictions, despite being slightly unconservative (+12.3% relative difference). This may be due to several factors including the presence of initial geometrical imperfections. With regards to the method 3, as outlined in the Eurocode 3, it is addressed for loads within the SLS range, and for such is already not yielding accurate results, once the considered load level is significantly higher than the SLS in the case of a 1.8 m beam.

7. Conclusions

This paper identifies the main challenges related to the development of a solution capable of being implemented as a continuous production for a foam-filled steel web sandwich panel for floor rehabilitation applications. With the proposed system, it is expected to foster the use of lightweight modular solutions in the rehabilitation of degraded structures, thus contributing to a reduction of generated wastes and minimizing raw materials consumption.

To tackle the industrial challenges identified during the manufacture of the panels, an alternative prototype for the flooring solution is conceived, and preliminarily assessed in a quasi-static flexural experimental campaign conducted on full-scale single and jointed panels. Hence, the obtained results are compared with the analytical design, to verify the fulfilment of both ULS and SLS requirements and the accuracy of the prescribed methods to predict the mechanical flexural response of the sandwich panels, as well as the mechanical contribution of the PUR foam core.

With regards to the continuous manufacturing process, the fixing of intermediary C and Z-shaped profiles (as webs) into the bottom face sheet of the panels represented a critical step due to their slenderness and consequent low-rigidity. The following version of the prototype, with the lateral webs being part of the bottom face sheet, clearly proved improving the overall consistency and quality control, as well as homogenous foaming of the cellular core.

When subjected to a four-point-bending test, the single panels (SP1 and SP2) started to deform due to wrinkling of the upper face sheet. Subsequently, with increasing load, the panels exhibited shear buckling of the vertical elements at the webs, specially at the support and the loading zone. At the end of the test, panel SP1 exhibited intensive plastic deformations distributed among one of the loading zones and the opposite support, while in panel SP2 plasticity was concentrated into a single loading zone, in which a plastic hinge was formed.

For the adhesively jointed panels (DP1 and DP2) assessed in four-point-bending test, failure also initiated with the wrinkling of the upper face sheet. Nevertheless, the tested panels failed at different load levels and with different plastic deformation evolution. For set of panels DP1, the two panels failed separately, with plasticity occurring primarily in a single panel, which only in a second stage was transferred to the next one. For set of panels DP2, plastic deformations progressed in a more even way among the connected panels, and failure was concentrated within one of the webs and the opposite loading zone region due to shear buckling. Nevertheless, both panels have shown adequate load-carrying capacity, higher than the predicted based on the single experimental results, even after sustained

plastic deformation. The difference observed on the behaviour of both sets of jointed panels highlights the importance of dimensional consistency, in order to guarantee an efficient load distribution among adjacent panels.

The estimated load-carrying capacity of the sandwich panels according to EN 1991-1-3 represented approximately 70% of the ultimate load observed on the experimental single panel tests. Furthermore, even after progressive deformation the panels satisfactorily preserve their load-carrying capacity, especially for the jointed panels.

In terms of SLS, the average vertical deflection measured at midspan when subjected to equivalent SLS load combination (approximately 0.2 mm) is substantially smaller than the maximum prescribed on the building codes for the same span length (7.2 mm). Moreover, disregarding the stabilizing effect of the PUR foam led to conservative predictions for the three assessed effective cross-sections. The most accurate estimation was obtained by accounting for the mechanical response of the gross cross-section (Method 1) of the sandwich panels (about +7% relative difference), whereas the Method 3 (described in the Eurocode) led to more conservative estimation (about +21% relative difference). In contrast, for load levels surpassing the SLS, although unconservative, Method 2 has proven to be the most precise, and led to the reasonably accurate prediction on the flexural stiffness of the panels (about +12% relative difference).

CRediT authorship contribution statement

Guilherme Gontijo: Formal analysis, Investigation, Writing – original draft. **Marco Abreu Filho:** Formal analysis, Investigation, Writing – review & editing. **Pier Giovanni Benzo:** Formal analysis, Investigation, Writing – review & editing. **João M. Pereira:** Conceptualization, Formal analysis, Funding acquisition, Investigation, Methodology, Project administration, Supervision, Validation, Writing – review & editing. **José Machado:** Conceptualization, Funding acquisition, Project administration, Validation, Writing – review & editing. **Zlatan Z. Denchev:** Funding acquisition, Supervision, Writing – review & editing. **José Sena-Cruz:** Conceptualization, Formal analysis, Funding acquisition, Investigation, Methodology, Supervision, Validation, Writing – review & editing.

Declaration of competing interest

The authors declare that they have no known competing financial interests or personal relationships that could have appeared to influence the work reported in this paper.

Data availability

Data will be made available on request.

Acknowledgements

This work was developed within the scope of the research project “Lightslab – Desenvolvimento de soluções inovadoras de lajes de painel sandwich”, supported by FEDER funds through the Operational Program for Operational Program for Competitiveness and Internationalization (POCI) and the Portuguese National Innovation Agency (ANI) – project no. 33865 [POCI-01-0247-FEDER-033865]. Furthermore, it was partly financed by FCT/MCTES through national funds (PIDDAC) under the R&D Unit Institute for Sustainability and Innovation in Structural Engineering (ISISE), under reference UIDB/04029/2020 (doi.org/10.54499/UIDB/04029/2020), and under the Associate Laboratory Advanced Production and Intelligent Systems ARISE under reference LA/P/0112/2020. The 1st, 2nd and 3rd authors wish also to acknowledge the grants 2021.07696.BD, 2022.13310.BD and DFA/BD/8319/2020 respectively, provided by Fundação para a Ciência e a Tecnologia, IP (FCT), financed by European Social Fund and national funds through the FCT/MCTES. Acknowledgments are extended to LEST – Laboratório de Estruturas, for their technical and material support

Annex A.

This section provides further details on the calculation procedures used to estimate the sandwich panels’ structural performance. The sandwich panel was designed according to the structural model of a simply supported beam subjected to a uniformly distributed load, as shown in Figure A1.

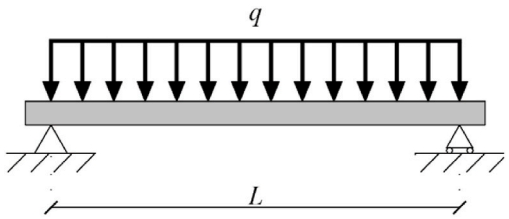

Fig. A1. Structural model adopted in the preliminary design stage.

The final prototype load carrying capacity (F_{ULS}) for the support and loading conditions described above is obtained from the bending moment diagram equation as follows:

$$F_{ULS} = \frac{8 \times M_{Rd}}{L^2} \tag{A1}$$

F_{ULS} was designed to be greater than the fundamental combination for the ULS verification (q_{uls}) given by Ref. [60]:

$$q_{ULS} = \gamma_g \times G_k + \gamma_Q \times Q_k \tag{A2}$$

where G_k is the characteristic value of the permanent actions (including self-weight of the panel and additional 1.5 kN/m^2 to account for the non-structural members, such as floor finishings), Q_k is the characteristic value of the variable action for residential buildings (set as 2.0 kN/m^2 for the current application), γ_G and γ_Q are the partial factors for the permanent actions and variable action, respectively. γG and γ_Q are set equal to 1.35 and 1.50 accordingly [60].

For what concerns the sandwich panel's stiffness, the maximum vertical deflection at midspan (δ_{max}) is given by:

$$\delta_{max} = \frac{q \times L^2}{584 \times E \times I_{eff}} \tag{A3}$$

where q is the uniformly distributed load applied to the beam, and I_{eff} is the moment of inertia of the effective cross-section estimated according to the EMW. The vertical deflection of the sandwich panel was verified for the characteristic combination at the SLS (q_{SLS}) given by Ref. [60]:

$$q_{SLS} = G_k + \psi_0 \times Q_k \tag{A4}$$

where ψ_0 is the factor for the characteristic value of the variable action for residential areas set equal to 0.7 [60].

The sandwich panel's stiffness was designed to fulfil the requirements imposed on the vertical deflection of generic floors in the national annex of the transposed Portuguese version of the Eurocode 3 Part 1-1 [62]. The total vertical deflection (δ_{max}) is the sum of the deflections due to the permanent actions (δ_1) and due to the variable action for residential buildings (δ_2). Since the bending stiffness of the sandwich panel depends on the stress level acting on it, two distinct I_{eff} shall be estimated for the different types of actions. Nevertheless, as a conservative hypothesis, both δ_1 and δ_2 were obtained considering the effective properties estimated considering the stress level corresponding to q_{sls}. Furthermore, in the preliminary design stage, I_{eff} was estimated considering the most conservative hypothesis on the influence of the foam stiffening effect on the structural performance of the panel, namely Method 2, described in Section 6.

To compare the result of the analytical design with the experimental results, it is necessary to adapt the analytical estimation to the structural model of the experimental setup. The flexural tests were conducted according to a four-point bending configuration, corresponding to a simply supported beam subjected to two concentrated forces ($F/2$) applied at thirds of the span, as illustrated in Figure A2.

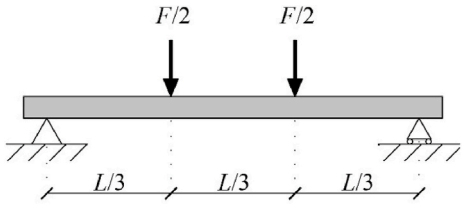

Fig. A2. Structural model of the four-point bending flexural test.

The estimation of the maximum bending moment (M_{EXP}) obtained during the test is obtained according to the following equation:

$$M_{EXP} = \frac{F_{EXP} \times L}{6} \tag{A5}$$

The ultimate load-carrying capacity of the sandwich panel estimated according to the Eurocode 3 Part 1–3 [54] for the structural model of the four-point bending test is determined by substituting M_{EXP} and F_{EXP} for M_{Rd} and F_{ULS}, respectively, in Equation (A5). The equation is then rearranged as shown below:

$$F_{ULS} = \frac{6 \times M_{Rd}}{L} \tag{A6}$$

Regarding the validation of the analytical design of the sandwich panel stiffness, firstly, the SLS load level corresponding to the structural model of the flexural test (F_{SLS}) is determined according to Equation (A6):

$$F_{SLS} = q_{SLS} \times L \tag{A6}$$

The experimental values of the deflection (δ_{exp}) may then be extracted from the load-displacement curve for the corresponding SLS load level.

The analytical prediction of the vertical midspan deflection and the bending stiffness is carried out according to three different approaches described in detail in Section 6, namely Method 1 (K_{M1}, δ_{M1}), Method 2 (K_{M2}, δ_{M2}), and Method 3 (K_{M3}, δ_{M3}). For a simply supported beam with two concentrated forces applied at thirds of the span, the midspan deflection can be calculated as follows:

$$\delta_{Mi} = \frac{23 \times F \times L^3}{1296 \times E \times I_{Mi}} \; with \; i = 1, 2, 3 \tag{A8}$$

where I_{M1} is the moment of inertia of the gross cross-section, I_{M2} is the moment of inertia of the effective cross-section considering the stress level corresponding to F_{SLS}, and I_{M3} is the moment of inertia of the effective cross-section using the interpolation method of the Eurocode 3 Part 1–3 [54]. Finally, the analytical prediction of the bending stiffness is obtained as follows:

$$K_{Mi} = \frac{1296 \times E \times I_{Mi}}{23 \times L^3} \; with \; i = 1, 2, 3 \tag{A9}$$

References

[1] L. Lima, E. Trindade, L. Alencar, M. Alencar, L. Silva, Sustainability in the construction industry: a systematic review of the literature, J. Clean. Prod. 289 (2021), https://doi.org/10.1016/j.jclepro.2020.125730.

[2] A. Ruuska, T. Häkkinen, Material efficiency of building construction, Buildings 4 (2014) 266–294, https://doi.org/10.3390/buildings4030266.

[3] P. Luechinger, J. Fischer, C. Christis, G. Dieteren, F. Landon, S. Leivestad, N. Malakatas, G. Mancini, J. Markova, S. Matthews, T. Nolan, C. Nuti, E. Osmani, G. Ronnow, S. Juergen, P. Tanner, Report EUR 27128 -new European technical rules for the assessment and retrofitting of existing structures, JCR Science and Policy Report (2015), https://doi.org/10.2788/052881.

[4] S. Navaratnam, A. Satheeskumar, G. Zhang, K. Nguyen, S. Venkatesan, K. Poologanathan, The challenges confronting the growth of sustainable prefabricated building construction in Australia: construction industry views, J. Build. Eng. 48 (2022), https://doi.org/10.1016/j.jobe.2021.103935.

[5] M. Norouzi, M. Chàfer, L.F. Cabeza, L. Jiménez, D. Boer, Circular economy in the building and construction sector: a scientific evolution analysis, J. Build. Eng. 44 (2021), https://doi.org/10.1016/j.jobe.2021.102704.

[6] S. Labò, E. Casprini, C. Passoni, J. Zanni, A. Belleri, A. Marini, P. Riva, Application of low-invasive techniques and incremental seismic rehabilitation to increase the feasibility and cost-effectiveness of seismic interventions, in: Procedia Structural Integrity, Elsevier B.V., 2018, pp. 185–193, https://doi.org/10.1016/j.prostr.2018.11.025.

[7] A. Marini, C. Passoni, P. Riva, P. Negro, E. Romano, F. Taucer, Technology options for earthquake resistant, eco-efficient buildings in Europe: Research needs (2014), https://doi.org/10.2788/68902.

[8] A. Elnokaly, A. Elseragy, Sustainable heritage development - learning from urban conservation of heritage projects in non-western contexts, Eur. J. Sustain. Dev. 2 (2013) 31–54, https://doi.org/10.14207/ejsd.2013.v2n1p31.

[9] A. Costa, J. Guedes, H. Varum, Structural Rehabilitation of Old Buildings, Springer, 2003.

[10] M. Branco, L.M. Guerreiro, Seismic rehabilitation of historical masonry buildings, Eng. Struct. 33 (2011) 1626–1634, https://doi.org/10.1016/j.engstruct.2011.01.033.

[11] M. Garrido, J.R. Correia, T. Keller, F.A. Branco, Adhesively bonded connections between composite sandwich floor panels for building rehabilitation, Compos. Struct. 134 (2015) 255–268, https://doi.org/10.1016/j.compstruct.2015.08.080.

[12] M. Kamali, K. Hewage, A.S. Milani, Life cycle sustainability performance assessment framework for residential modular buildings: aggregated sustainability indices, Build. Environ. 138 (2018) 21–41, https://doi.org/10.1016/j.buildenv.2018.04.019.

[13] P.S.P. Wong, C. Zwar, E. Gharaie, Examining the drivers and states of organizational change for greater use of prefabrication in construction projects, J. Construct. Eng. Manag. 143 (2017), https://doi.org/10.1061/(asce)co.1943-7862.0001309.

[14] J. Zhou, D. Ren, A hybrid model of external environmental benefits compensation to practitioners for the application of prefabricated construction, Environ. Impact Assess. Rev. 81 (2020), https://doi.org/10.1016/j.eiar.2019.106358.

[15] Y.H. Lee, C.S. Tan, S. Mohammad, M. Tahir, P.N. Shek, Review on cold-formed steel connections, Sci. World J. 2014 (2014), https://doi.org/10.1155/2014/951216.

[16] M. Mastali, I.B. Valente, J.A.O. Barros, D.M.F. Gonçalves, Development of innovative hybrid sandwich panel slabs: experimental results, Compos. Struct. 133 (2015) 476–498, https://doi.org/10.1016/j.compstruct.2015.07.114.

[17] T. Sharaf, A. Fam, Analysis of large-scale cladding sandwich panels composed of GFRP skins and ribs and polyurethane foam core, Thin-Walled Struct. 71 (2013) 91–101, https://doi.org/10.1016/j.tws.2013.05.006.

[18] J.M. Davies, Lightweigth Sandwich Construction, John Wiley & Sons, New York, USA, 2008.

[19] D. Gay, Suong V. Hoa, S.W. Tsai, Composite Materials: Design and Applications, CRC Press, 2003.

[20] S. Aimmanee, J.R. Vinson, Analysis and optimization of foam-reinforced web core composite sandwich panels under in-plane compressive loads, J. Sandw. Struct. Mater. 4 (2003), https://doi.org/10.1106/109963602021030.

[21] W. Qiao, X. Yan, R. Zhu, F. Wang, D. Wang, Flexural properties of new cold-formed thin-walled steel and concrete composite slabs, J. Build. Eng. 31 (2020) 101441, https://doi.org/10.1016/j.jobe.2020.101441.

[22] M.F. Hassanein, M. Elchalakani, A.A. Elkawas, Thin-Walled Structures Design of cold-formed CHS braces for steel roof structures, Thin-Walled Struct. 120 (2017) 249–259, https://doi.org/10.1016/j.tws.2017.09.002.

[23] M. Elchalakani, X.L. Zhao, R. Grzebieta, Bending tests to determine slenderness limits for cold-formed circular hollow sections, J. Constr. Steel Res. 58 (2002) 1407–1430, https://doi.org/10.1016/S0143-974X(01)00106-7.

[24] N. Pokharel, M. Mahendran, Experimental investigation and design of sandwich panels subject to local buckling effects, J. Constr. Steel Res. 59 (2005) 1533–1552, https://doi.org/10.1016/S0143-974X(03)00084-1.

[25] M.A. Dar, N. Subramanian, A.R. Dar, A.F. Ghowsi, F. Sidiqui, S. Fayaz, M.S. Mir, Comparison of various shear connectors for improved structural performance in CFS concrete composite slabs, Eng. Struct. 220 (2020) 111008, https://doi.org/10.1016/j.engstruct.2020.111008.

[26] R. Sagadevan, B.N. Rao, Experimental and analytical study on structural performance of polyurethane foam-filled built-up galvanized iron members, Thin-Walled Struct. 146 (2020) 106446, https://doi.org/10.1016/J.TWS.2019.106446.

[27] C.R. Briscoe, S.C. Mantell, T. Okazaki, J.H. Davidson, Local shear buckling and bearing strength in web core sandwich panels: model and experimental validation, Eng. Struct. 35 (2012) 114–119, https://doi.org/10.1016/J.ENGSTRUCT.2011.10.020.

[28] G. Carbonari, S. Cavalaro, M.M. Cansario, A. Aguado, Flexural behaviour of light-weight sandwich panels composed by concrete and EPS, Construct. Build. Mater. 35 (2012) 792–799, https://doi.org/10.1016/j.conbuildmat.2012.04.080.

[29] X. Zhou, Y. Shi, L. Xu, X. Yao, W. Wang, A simplified method to evaluate the flexural capacity of lightweight cold-formed steel floor system with oriented strand board subfloor, Thin-Walled Struct. 134 (2019) 40–51, https://doi.org/10.1016/j.tws.2018.09.006.

[30] S. Gopinath, V. Ramesh Kumar, H. Sheth, A. Ramachandra Murthy, N.R. Iyer, Prefabricated sandwich panels using cold-formed steel and textile reinforced concrete, Construct. Build. Mater. 64 (2014) 54–59, https://doi.org/10.1016/j.conbuildmat.2014.04.068.

[31] H. Güldür, E. Baran, C. Topkaya, Experimental and numerical analysis of cold-formed steel floor trusses with concrete filled compression chord, Eng. Struct. 234 (2021), https://doi.org/10.1016/j.engstruct.2020.111813.

[32] J. Ye, W. Chen, Z. Wang, Fire-resistance behavior of a newly developed cold-formed steel composite floor, J. Struct. Eng. 143 (2017), https://doi.org/10.1061/(asce)st.1943-541x.0001744.
[33] P. Kyvelou, L. Gardner, D.A. Nethercot, Testing and analysis of composite cold-formed steel and Wood−Based flooring systems, J. Struct. Eng. 143 (2017), https://doi.org/10.1061/(asce)st.1943-541x.0001885.
[34] L. min Tian, Y. feng Kou, J. ping Hao, L. wei Zhao, Flexural performance of a lightweight composite floor comprising cold-formed steel trusses and a composite mortar slab, Thin-Walled Struct. 144 (2019), https://doi.org/10.1016/j.tws.2019.106361.
[35] J.Y.R. Liew, Y.S. Chua, Z. Dai, Steel concrete composite systems for modular construction of high-rise buildings, Structures 21 (2019) 135–149, https://doi.org/10.1016/j.istruc.2019.02.010.
[36] J. Ryu, Y.Y. Kim, M.W. Park, S.W. Yoon, C.H. Lee, Y.K. Ju, Experimental and numerical investigations of steel-polymer hybrid floor panels subjected to three-point bending, Eng. Struct. 175 (2018) 467–482, https://doi.org/10.1016/j.engstruct.2018.08.030.
[37] M.J. Park, Y.K. Ju, Finite element model for the steel-polymer composite floor filled with phase-change amorphous polymers at elevated temperatures, Construct. Build. Mater. 319 (2022), https://doi.org/10.1016/j.conbuildmat.2021.126059.
[38] M.J. Park, S.W. Yoon, Y.K. Ju, New approaches for floor vibrations of steel–polymer–steel sandwich floor systems, Eng. Struct. 258 (2022), https://doi.org/10.1016/j.engstruct.2022.114141.
[39] H. Abdolpour, J. Garzón-Roca, G. Escusa, J.M. Sena-Cruz, J.A.O. Barros, I.B. Valente, Development of a composite prototype with GFRP profiles and sandwich panels used as a floor module of an emergency house, Compos. Struct. 153 (2016) 81–95, https://doi.org/10.1016/j.compstruct.2016.05.069.
[40] X. Zhao, L. Tan, F. Zhang, Mechanical behavior of sandwich panels with hybrid PU foam core, Adv. Civ. Eng. 2020 (2020), https://doi.org/10.1155/2020/2908054.
[41] K. Thomas, H. Christoph, V. Till, Structural concept, design, and experimental verification of a glass fiber-reinforced polymer sandwich roof structure, J. Compos. Construct. 12 (2008) 454–468, https://doi.org/10.1061/(ASCE)1090-0268(2008)12:4(454).
[42] D. Zenkert, N.I. Fund, The Handbook of Sandwich Construction, Engineering Materials Advisory Services, 1997.
[43] M. Garrido, J.F.A. Madeira, M. Proença, J.R. Correia, Multi-objective optimization of pultruded composite sandwich panels for building floor rehabilitation, Construct. Build. Mater. 198 (2019) 465–478, https://doi.org/10.1016/j.conbuildmat.2018.11.259.
[44] T.L. Silva, I.B. Valente, J. Barros, M.J. Roupar, S.M. Silva, R. Mateus, Thermal performance of steel and fibre reinforced concrete composite floor, in: RILEM Spring Convention 2020 – Ambitioning a Sustainable Future for Built Environment: Comprehensive Strategies for Unprecedented Challenges, Guimarães, 2020.
[45] J.R. Correia, F.A. Branco, J. Ferreira, GFRP-concrete hybrid cross-sections for floors of buildings, Eng. Struct. 31 (2009) 1331–1343, https://doi.org/10.1016/j.engstruct.2008.04.021.
[46] H. Lovon, V. Silva, R. Vicente, T.M. Ferreira, A.A. Costa, Characterisation of the masonry building stock in Portugal for earthquake risk assessment, Eng. Struct. 233 (2021), https://doi.org/10.1016/j.engstruct.2021.111857.
[47] M. Mastali, I.B. Valente, J.A.O. Barros, Development of innovative hybrid sandwich panel slabs: Advanced numerical simulations and parametric studies, Compos. Struct. 152 (2016) 362–381, https://doi.org/10.1016/j.compstruct.2016.05.072.
[48] P.G. Benzo, J.M. Pereira, J. Sena-Cruz, Optimization of steel web core sandwich panel with genetic algorithm, Eng. Struct. 253 (2022) 113805, https://doi.org/10.1016/j.engstruct.2021.113805.
[49] Z.K. Awad, T. Aravinthan, Y. Zhuge, A. Manalo, Geometry and restraint effects on the bending behaviour of the glass fibre reinforced polymer sandwich slabs under point load, Mater. Des. 45 (2013) 125–134, https://doi.org/10.1016/j.matdes.2012.08.072.
[50] G. Zhang, B. Wang, L. Ma, L. Wu, S. Pan, J. Yang, Energy absorption and low velocity impact response of polyurethane foam filled pyramidal lattice core sandwich panels, Compos. Struct. 108 (2014) 304–310, https://doi.org/10.1016/j.compstruct.2013.09.040.
[51] G.B.G. Ananthi, K. Roy, K. Ghosh, K. Poologanathan, J.B.P. Lim, An investigation on stiffened cold-formed steel unequal angle box section columns, J. Build. Eng. 76 (2023) 106989, https://doi.org/10.1016/j.jobe.2023.106989.
[52] L. Xu, P. Sultana, X. Zhou, Flexural strength of cold-formed steel built-up box sections, Thin-Walled Struct. 47 (2009) 807–815, https://doi.org/10.1016/j.tws.2009.01.005.
[53] Y.L. Li, Y.Q. Li, Z.Y. Shen, Investigation on flexural strength of cold-formed thin-walled steel beams with built-up box section, Thin-Walled Struct. 107 (2016) 66–79, https://doi.org/10.1016/j.tws.2016.05.026.
[54] European Committee for Standardization, EN 1993-1.2 Design of Steel Structures. General Rules. Structural Fire Design, EN 1993-1.3 Design of Steel Structures, General Rules. Supplementary rules for cold-formed members and sheeting, Brussels, Belgium, 2005.
[55] X. Yao, X. Zhou, Y. Shi, Y. Guan, Y. Zou, Simplified calculation method for flexural moment capacity of cold-formed steel built-up section beams, Adv. Struct. Eng. 23 (2020) 3153–3167, https://doi.org/10.1177/1369433220931208.
[56] AISI, S100-16 North American Specification for the Design of Cold-Formed Steel Structural Members, American Iron and Steel Institute, Washington DC, 2016.
[57] GB 50018-2002, Technical Code of Cold-Formed Thin-Walled Steel Structures, Ministry of Construction of the P.R. China, Beijing, 2002.
[58] J. Ye, S.M. Mojtabaei, I. Hajirasouliha, P. Shepherd, K. Pilakoutas, Strength and deflection behaviour of cold-formed steel back-to-back channels, Eng. Struct. 177 (2018) 641–654, https://doi.org/10.1016/j.engstruct.2018.09.064.
[59] European Committee for Standardization, EN 1993-1-5:2006. Eurocode 3: Design of Steel Structures - Part 1-5, Plated structural elements, 2006.
[60] European Committee for Standardization, EN 1990:2002. Eurocode 0 - Basis of Structural Design, 2002.
[61] European Committee for Standardization, EN 1991-1-1:2002. Eurocode 1: Actions on Structures - Part 1-1: General Actions - Densities, Self-Weight, Imposed Loads for Buildings, 2002.
[62] European Committee for Standardization, NP EN 1993-1-1:2010. Eurocódigo 3 - Projecto de estruturas de aço - Parte 1-1: Regras gerais e regras para edifícios, 2010.
[63] M. Abreu Filho, G.L. Gontijo, S.C. Oliveira, P.G. Benzo, A. Dushimimana, Z.Z. Denchev, J.M. Pereira, J. Sena-Cruz, Influence of temperature and different post curing conditions on the mechanical behaviour of polyurethane-based adhesive for civil engineering applications, in: Proceedings of the 20th European Conference on Composite Materials - Composites Meet Sustainability, EPFL Lausanne, Composite Construction Laboratory, Lausanne, 2022, pp. 820–827.
[64] A. Benedetti, P. Fernandes, J.L. Granja, J. Sena-Cruz, M. Azenha, Influence of temperature on the curing of an epoxy adhesive and its influence on bond behaviour of NSM-CFRP systems, Compos. B Eng. 89 (2016) 219–229, https://doi.org/10.1016/j.compositesb.2015.11.034.
[65] E. Ellobody, R. Feng, B. Young, Chapter 3 - finite element modeling, in: E. Ellobody, R. Feng, B. Young (Eds.), Finite Element Analysis and Design of Metal Structures, Butterworth-Heinemann, Boston, 2014, pp. 31–55, https://doi.org/10.1016/B978-0-12-416561-8.00003-2.
[66] P. Kyvelou, L. Gardner, D.A. Nethercot, Finite element modelling of composite cold-formed steel flooring systems, Eng. Struct. 158 (2018) 28–42, https://doi.org/10.1016/j.engstruct.2017.12.024.
[67] M. Proença, M. Garrido, J. Correia, G. Escusa, J. Sena-Cruz, Preliminary Design of the Easyfloor Sandwich Panel. Task 1.1, Report 1.1 - ANI - EASYFLOOR - Development of Innovative Sandwich Panels Made of Fibre Reinforced Polymer (FRP) for the Rehabilitation of Degraded Wooden Floors of Old Buildings 2016, 2016.
[68] J. Machado, P. Benzo, M. Abreu Filho, A. Dushimimana, G. Gontijo, M. Abreu Filho, J. Sena-Cruz, J. Pereira, M. Silva, P. Lourenço, Design of the LightSlab sandwich panel, in: Report 6.3 - ANI - LightSlab - Desenvolvimento de soluções inovadoras de lajes de painel sandwich 2022, 2022.
[69] P.G. Benzo, J.M. Pereira, J. Sena-Cruz, Structural response of steel sandwich panels with PUR foam core subjected to edgewise compression: experimental, numerical, and analytical considerations, Construct. Build. Mater. 409 (2023) 134009, https://doi.org/10.1016/j.conbuildmat.2023.134009.